32nd International Conference
ENGINEERING MECHANICS 2026
Medlov, Czech Republic, May 11 – 13, 2026

MICROMECHANICAL PROPERTIES OF STEEL CORROSION PRODUCTS

Němeček J.[1], **Prošek Z.**[2], **Lukeš J.**[3], **Němeček J.**[4]

Abstract:
The micromechanical properties of the steel corrosion layer formed in cement paste under accelerated conditions were investigated using micro-pillar compression. Micro-pillars were fabricated by Xe plasma focused ion beam and tested in situ using a picoindenter. The results show clear mechanical degradation of the corrosion products compared to the original steel rod, manifested by reduced yield strength, peak stress, elastic modulus, and strain at peak stress. Additionally, the corrosion products exhibit less ductility and sudden failure during compression after reaching the maximum load.

Keywords: Steel corrosion, Micro-pillar, Focused ion beam, Accelerated test

1. Introduction

Corrosion of steel reinforcement is a problem in many building structures exposed to environmental influences such as moisture and ion transport. In a freshly cast concrete structure, the steel is protected from corrosion by a thin oxide layer, which causes the steel to be in a passive state and corrosion occurs at a significantly lower rate. The passive layer is maintained by the high pH of the concrete (pH>12). If the pH is reduced, for example by carbonation of the concrete (pH<10) or by the presence of chlorides from de-icing agents, then the passive layer is disrupted and corrosion occurs, often in localized places, later even over the entire surface of the reinforcement. Active corrosion, in the presence of moisture and oxygen, causes the formation of a series of hydroxides and oxides around the reinforcement, resulting in cracks in the concrete and ultimately the covering layer falling off. The main corrosion products found with X-ray diffraction (XRD) measurements were iron oxides (FeO, $\alpha - Fe_2O_3$, Fe_3O_4) and iron hydroxy-oxides ($\alpha, \beta, \gamma, \delta - FeOOH$). The rust layer exhibits also increased porosity compared to original metal (Zhao et al., 2011).

Due to a number of influencing factors, the mechanical properties of corrosion products show a significant dispersion of values in the literature (Zhao and Jin, 2016). In addition, their measurement requires special procedures in layers of only a few micrometers, which leads to the use of microscopic methods (Němeček et al., 2016; Shahrin and Bobko, 2019). These data provide essential inputs for numerical models that simulate the corrosion process (Korec et al., 2023, 2024). For examination of corrosion products, accelerated tests can be used, where the formation of corrosion products is controlled by an impressed corrosion current (Zhang et al., 2019; Andrade, 2023). This work, therefore, focuses on the characterization of corrosion products in a thin corrosion layer prepared in an accelerated test under galvanostatic conditions using scanning electron microscopy (SEM) and nanoindentation.

[1] Ing. Jiří Němeček, Ph.D., Orcid 0000-0002-5635-695X: Department of Mechanics, Faculty of Civil Engineering, Czech Technical University, Thákurova 2077/7; 166 29, Prague 6; CZ, jiri.nemecek.1@fsv.cvut.cz
[2] Doc. Ing. Zdeněk Prošek, Ph.D.: Department of Mechanics, Faculty of Civil Engineering, Czech Technical University, Thákurova 2077/7; 166 29, Prague 6; CZ, zdenek.prosek@fsv.cvut.cz
[3] Ing. Jaroslav Lukeš, Ph.D.: Division of biomechanics, Faculty of Mechanical Engineering, Czech Technical University, Technická 1902/4; 166 29, Prague 6; CZ, jaroslav.lukes@fs.cvut.cz
[4] Prof. Ing. Jiří Němeček, Ph.D., DSc., Orcid 0000-0002-3565-8182: Department of Mechanics, Faculty of Civil Engineering, Czech Technical University, Thákurova 2077/7; 166 29, Prague 6; CZ, jiri.nemecek@fsv.cvut.cz

ISSN: 1805-8256, doi: 10.21495/em2026-85

2. Experiments and methods

To conduct accelerated steel corrosion tests, cylindrical samples with a diameter of 27 mm and a height of 70 mm were fabricated and filled with cement paste.The mixture was prepared from Portland cement CEM I 42.5R with a water/cement ratio of 0.4 and the addition of 1% NaCl relative to the weight of cement. A 3 mm structural steel rod (cold-formed low carbon steel H9 S235JRC+C) was placed in the middle of the cylinder, 10 mm from the bottom, while the upper part of the rod was protected with an electrical insulation. After the fabrication the samples were stored in lime-saturated water for 14 days.

After curing, the samples were placed in an electrolytic cell with DC power source, where the positive pole of the source was connected to the reinforcement and the negative pole was connected to a stainless steel mesh electrode placed around the circumference of the sample at a distance of approximately 5 mm. The cell space was filled with electrolyte in the form of 0.3 M NaOH. The source maintained a constant current flowing through the reinforcement with a prescribed nominal current density of $500\,\mu A/cm^2$ for a duration of 3 days. This procedure led to a massive increase in corrosion products on the surface of the reinforcement and the formation of cracks in the direction from the reinforcement to the surface.

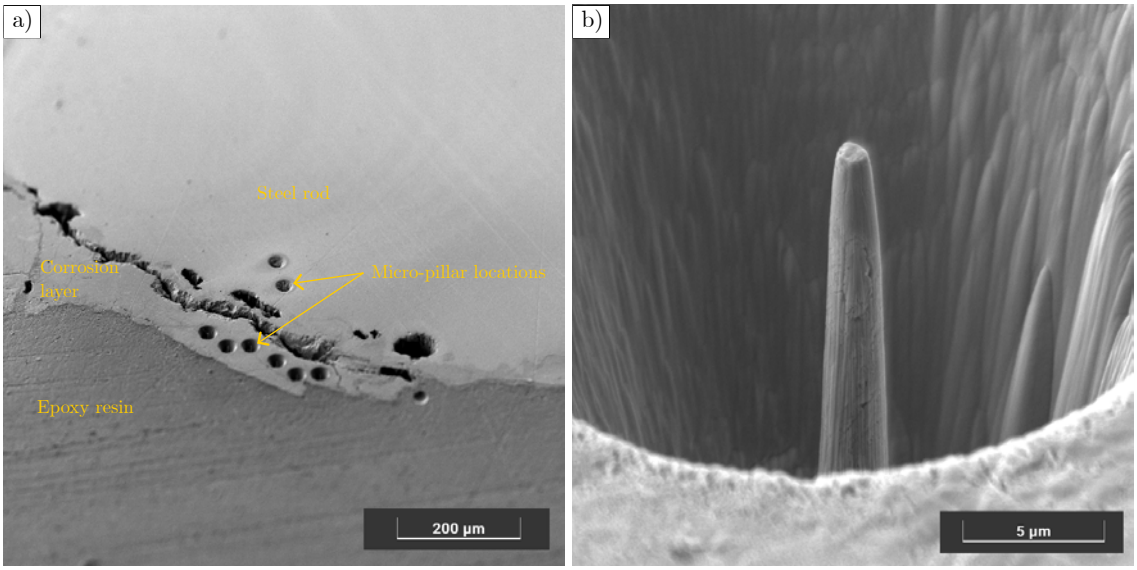

Fig. 1: SEM-SE images of (a) sample overview showing locations of the corrosion layer and fabricated micro-beams, (b) example of a fabricated micro-beam in the corrosion layer.

After the accelerated test, the samples were cut into thinner slices, dried at $50\,^{\circ}C$ for 1 day, and then embedded in epoxy resin to stabilize the corrosion layer formed around the steel rod during the polishing. The samples were subsequently polished using silicon carbide papers following the procedure described in Němeček et al. (2020). An example of a polished surface at the steel rod with the corrosion layer is shown in Fig. 1a. A Phenom XL desktop SEM was used to characterize the corrosion layer by EDS mapping over an area of $163\,\mu m^2$. The measurements were performed at an accelerating voltage of 15 kV.

A Tescan Amber X microscope was used to fabricate micro-pillars with Xe plasma focused ion beam (FIB) positioned primarily in the corrosion layer, as shown in Fig. 1a. FIB milling was performed with an accelerating voltage of 30 kV and decreasing current values from 10 nA to 250 pA when approaching the micro-pillar. An example of a fabricated pillar in the corrosion layer is shown in Fig. 1b. The dimensions of the micro-pillar are $\sim 12\,\mu m$ in height, $\sim 1.1\,\mu m$ at the top diameter, and $\sim 2.5\,\mu m$ at the bottom diameter. Then, a Hysitron PI-89 SEM PicoIndenter was used to compress the micro-pillars with diamond conical tip with a flat end with a radius of $5\,\mu m$. The loading was performed under displacement control up to a maximum displacement of 2000 nm, with a constant loading rate of 100 nm/s.

2.1. Results and discussion

The SEM characterization is shown in Fig. 2, which also shows the elemental composition (EDS maps) of the steel-corrosion layer transition region. The corrosion layer is clearly distinguishable in the BSE image (Fig. 2a), forming an irregular shape compared with the original steel rod. EDS mapping shows a

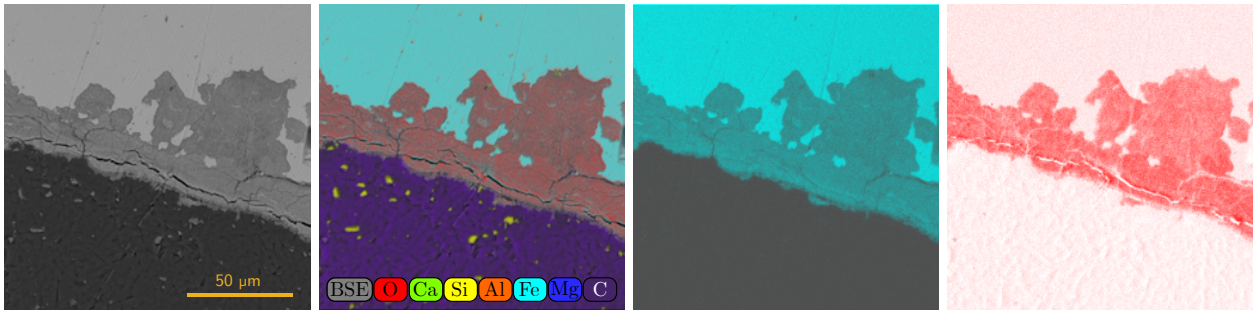

(a) Original BSE image. (b) EDS combined map. (c) Iron map. (d) Oxygen map.

Fig. 2: Characterization of steel-corrosion layer-epoxy resin by EDS mapping. a) Original BSE image, b) EDS combined map, c) Iron map, d) Oxygen map.

reduced iron content and a simultaneous increase in oxygen, confirming the formation of new corrosion products. However, precise phase identification requires complementary methods, such as XRD or Raman spectroscopy (Mi et al., 2023). Additionally, no Ca or Si was detected in the corrosion layer, indicating no intermixing with the surrounding cement paste.

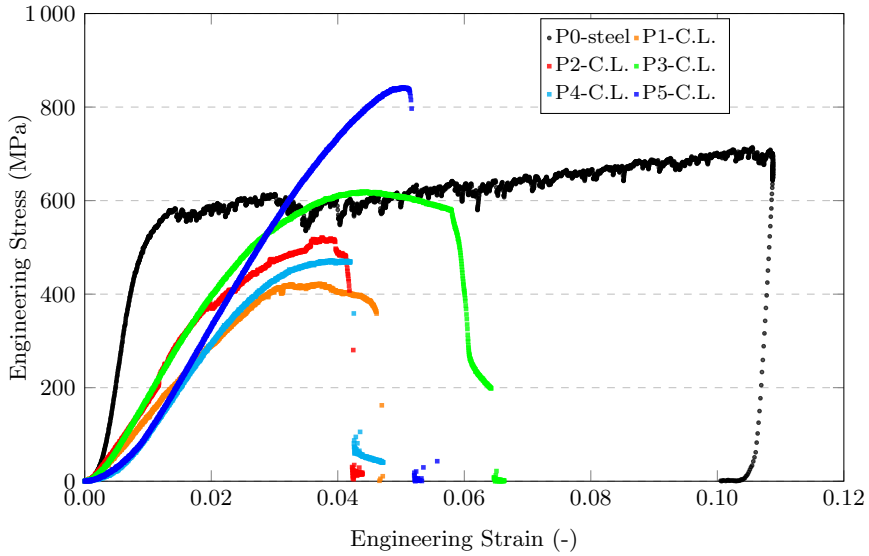

Fig. 3: Measured stress–strain curves from micro-pillar compression in the corrosion layer (C.L.) and in the steel rod.

The engineering stress-strain response from micro-pillar compression is presented in Fig. 3. The reference pillar fabricated in the steel rod exhibits behavior characterized by an initial linear elastic regime, followed by yielding and stable plastic flow with noticeable strain hardening, reaching a peak stress of 714 MPa. Since the pillar did not undergo a complete fracture during compression, the unloading segment follows an approximately linear elastic path. In contrast, micro-pillars prepared in the corrosion layer show an initial elastic response, followed by limited plastic deformation, followed by a rupture or instability. After reaching the peak stress, all corrosion-layer pillars undergo abrupt stress drops associated with sudden failure. The peak strength and failure strain vary among pillars, indicating pronounced microstructural heterogeneity. The evaluated mechanical properties are summarized in Table 1. The mechanical parameters generally reveal a decrease in the values for the corrosion products compared to the original steel. The corrosion layer exhibits a lower average yield strength (478 ± 126 MPa) and peak stress (575 ± 148 MPa) than the steel pillar (535 MPa and 714 MPa, respectively). The strain at peak stress is significantly smaller for corrosion products (0.041 ± 0.005) compared to the steel pillar (0.105) which is a consequence of the greater brittleness of corrosion products compared to the ductile steel. It is worth noting that the size of the reference steel pillar is probably smaller than the size of the ferrite grain (α-Fe). Ferrite in S235JRC+C steels occupies approximately 90% of the volume, is anisotropic with a grain size of around 20 μm. The reference value is therefore not a unique value for differently oriented grains and in further studies it would

be appropriate to perform measurements for more orientations, or possibly for a larger size, which would lead to the determination of the average properties of the steel for a larger volume.

The most significant reduction is observed in the elastic modulus. It should be noted that these values are most likely underestimated due to imperfect contact between the tip and the end of the pillar or other geometric inaccuracies. For a more accurate evaluation, further optimization of the micro-pillar geometry along with the application of a cyclic loading protocol would be necessary (Shahrin and Bobko, 2019).

Tab. 1: Parameters measured during micro-pillar compression.

Parameter	Steel (1 test)	Corrosion products (5 tests)	Change (%)
Yield Strength (MPa)	535	478 ± 126	-10.6
Peak Stress (MPa)	714	575 ± 148	-19.5
Elastic Modulus (GPa)	84.8	20.3 ± 2.5	-76.0
Strain at Peak Stress (-)	0.105	0.041 ± 0.005	-61.0

3. Conclusions

The micro-pillar compression results performed in this study demonstrate a clear mechanical degradation of the corrosion products compared to the steel substrate. While the pillar in steel exhibits significant ductility and high load-bearing capacity, the pillars in corrosion-layer show reduced strength, significantly lower stiffness, and limited deformability, followed by premature, unstable failure. The large scatter in the corrosion-layer response reflects pronounced microstructural heterogeneity.

Acknowledgments

This work was financially supported by the Czech Science Foundation under grant number 26-22195S and the Grant Agency of the Czech Technical University in Prague (SGS25/083/OHK1/2T/11). The authors also acknowledge the support of the Laboratory of Special Microscopy, Faculty of Civil Engineering, CTU in Prague.

References

Andrade, C. (2023) Steel corrosion rates in concrete in contact to sea water. *Cement and Concrete Research*, 165, pp. 107085.

Korec, E., Jirásek, M., Wong, H., and Martínez-Pañeda, E. (2023) A phase-field chemo-mechanical model for corrosion-induced cracking in reinforced concrete. *Construction and Building Materials*, 393, pp. 131964.

Korec, E., Jirásek, M., Wong, H., and Martínez-Pañeda, E. (2024) Unravelling the interplay between steel rebar corrosion rate and corrosion-induced cracking of reinforced concrete. *Cement and Concrete Research*, 186, pp. 107647.

Mi, T., Wang, J., McCague, C., and Bai, Y. (2023) Application of raman spectroscopy in the study of the corrosion of steel reinforcement in concrete: A critical review. *Cement and Concrete Composites*, 143, pp. 105231.

Němeček, J., Lukeš, J., and Němeček, J. (2020) High-speed mechanical mapping of blended cement pastes and its comparison with standard modes of nanoindentation. *Materials Today Communications*, 23, pp. 100806.

Němeček, J., Králík, V., Šmilauer, V., Polívka, L., and Jäger, A. (2016) Tensile strength of hydrated cement paste phases assessed by micro-bending tests and nanoindentation. *Cement and Concrete Composites*, 73, pp. 164–173.

Shahrin, R. and Bobko, C. (2019) Micropillar compression investigation of size effect on microscale strength and failure mechanism of calcium-silicate-hydrates (C-S-H) in cement paste. *Cement and Concrete Research*, 125, pp. 105863.

Zhang, W., Chen, J., and Luo, X. (2019) Effects of impressed current density on corrosion induced cracking of concrete cover. *Construction and Building Materials*, 204, pp. 213–223.

Zhao, Y. and Jin, W. (2016) Chapter 2 - steel corrosion in concrete. In Zhao, Y. and Jin, W., eds, *Steel Corrosion-Induced Concrete Cracking*, Butterworth-Heinemann, pp. 19–29.

Zhao, Y., Ren, H., Dai, H., and Jin, W. (2011) Composition and expansion coefficient of rust based on x-ray diffraction and thermal analysis. *Corrosion Science*, 53, 5, pp. 1646–1658.